Sensors and Materials, Vol. 37, No. 1 (2025) 13–22
MYU Tokyo

S & M 3888

A Fabry–Pérot Sensing Setup Based on a Coreless Fiber for the Measurement of Ethanol Concentration in Water-based Solutions

Marco Bianchetti,[1*] Brayan Kevin Aviles-Diaz,[1] Maria Susana Avila-Garcia,[1]
Maria Elena Sosa-Morales,[2] Roberto Rojas-Laguna,[3]
Juan Manuel Sierra-Hernandez,[3] and Stefano Toffanin[4]

[1]Departamento de Estudios Multidisciplinarios, Universidad de Guanajuato,
Avenida Universidad S/N, Yuriria, Guanajuato 38944, México
[2]Departamento de Alimentos, Universidad de Guanajuato,
Ex Hacienda El Copal, Irapuato, Guanajuato 36500, México
[3]Departamento de Ingeniería Electrónica, Universidad de Guanajuato,
Carretera Salamanca Valle de Santiago, Salamanca, Guanajuato 36787, México
[4]Istituto per lo Studio dei Materiali Nanostrutturati, CNR, Via P. Gobetti, Bologna 40129, Italy

(Received September 20, 2024; accepted November 21, 2024)

Keywords: ethanol, Fabry–Pérot, fiber optics, sensors, wine

Ethanol solutions are present in many industries, including the beverage, medical, and fuel industries. While electrical methods for measuring the ethanol concentration in solutions are subject to electromagnetic interference, may require large amounts of solution, or take a long time, optical techniques based on fiber optics are immune to electromagnetic interference, are chemically inert, and can deliver signals over long distances with minimal noise. However, fiber optic sensors often require expensive equipment to manufacture, e.g. a CO_2 laser for manufacturing Bragg gratings, or expensive photonic crystal fibers, and often are difficult to assemble. In this paper, we propose a coreless-fiber-based Fabry–Pérot sensor that is very easy to manufacture; then, we tested and calibrated it in solutions of n% ethanol in deionized water at temperatures of 23, 21, and 19 °C in the range n = 0−15 typical in the wine industry. The manufactured interferometers worked either by shifting the minimum of a valley at a rate of 0.07630 nm/n or by decreasing the intensity of the measured signal (absorption) at a rate of −0.15696 dBm/n in the entire range n = 0−15.

1. Introduction

Ethanol is a common substance that is used as a solvent in industrial processes, in the medical and beverage industries, and as a potential additive to fuel in the car industry. It is a colorless substance that easily dissolves in water and other organic solvents, and reliable and fast methods to measure its concentration are needed.(1)

Non-optical measurement methods for ethanol concentration have several disadvantages: e.g., the need for calibration, often time-consuming and inaccurate, expensive, and wastage of

*Corresponding author: e-mail: mb@ugto.mx
https://doi.org/10.18494/SAM5310

ISSN 0914-4935
https://myukk.org/

large amounts of products. On the other hand, optical methods are immune to electromagnetic interference; in particular, fiber-optic-based sensors are chemically inert, can deliver an optical signal through a long distance with minimal loss of quality, and are light and noninvasive.

A recent review on fiber optic ethanol sensors in water solution was written by Memon *et al.*[2] In this review, the sensors are divided into three main groups: absorption, surface-modified, and Bragg grating sensors. However, the production of such devices is often complicated and requires specialized equipment. For example, a taper-based sensor requires a tapering machine, and the resulting sensor is extremely fragile given its diameter range of 10–50 mm, surface-modified sensors require expensive equipment to coat the fiber surface and to control the thickness of the deposited material, and fiber Bragg gratings require a CO_2 laser to inscribe the gratings in the core of the fiber.

Thirunavakkarasu *et al.* deposited a thin layer (45 nm) of Au on a thinned fiber Bragg grating (FBG) to increase its sensitivity when immersed in ethanol solutions with a concentration range of 0–100% and reported a sensitivity of 20 pm/refractive index unit (pm/RIU).[3]

Cano-Velázquez *et al.* proposed a temperature-compensated sensor for determining the concentration of ethanol in water.[4] They transferred two photonic crystals onto the tips of two fiber optics. One fiber tip was covered with a polymer and does not come in contact with the surrounding liquid, and is therefore sensitive to only the solution's temperature, whereas the other is in direct contact with the liquid, and is therefore sensitive to both the temperature and concentration of the solution. Combining the information obtained from the two fiber tips, they authors achieved a sensitivity of 0.053 nm/% in the temperature range of 25−60 °C and the concentration range of 0−60%.[4]

Marfu'ah *et al.* used a multimode–single-mode–multimode (MSM) fiber structure in which the core of the multimode (MM) fiber launches light into the cladding of the single-mode (SM) fiber and then rejoins the larger core of the MM fiber.[5] While traveling in the SM cladding, the light can interact with a water–ethanol solution via the evanescent wave. The light source emits at 1310 nm with a power output of about −6 dBm. To enhance the performance of the sensor, they coated the MSM fiber structure with Novolac resin, obtaining a sensitivity of 0.028972 dBm/%.[5]

In the study by Tian *et al.*, a Fabry–Pérot sensor with a concave tip manufactured with a photonic crystal fiber achieved a sensitivity of 1636.62 nm/RIU when immersed in a solution of ethanol in water in the range of 0−19.11% in weight. The concave shape helps the liquid enter the cavities of the photonic fiber when the sensor is immersed in the solution.[6]

Sensors that do not require a continuous immersion in a liquid solution can also be designed. In the study by Paixão *et al.*, a Fabry–Pérot sensor manufactured with a photonic fiber can detect the presence of a solvent by suspending the tip of the sensor in the vapor above the liquid. However, they reported a waiting time of 90 min to allow the solvent vapor to enter the photonic fiber hollow cavities and achieve stabilization, and observe the temperature dependence of the measurements.[7]

Naku *et al.* developed a Fabry–Pérot sensor used by immersing into and withdrawing from a solution the tip of a cleaved SMF, thereby creating a suspended droplet.[8] By analyzing the

signal delivered by the Fabry–Pérot sensor to a photodiode with a machine learning algorithm, they could discern between various solvents.[8]

In this work, we propose an ethanol sensor based on a Fabry–Pérot interferometer to be immersed in a water–ethanol solution, which is very easy and simple to manufacture compared with those reported previously, and that does not need any specialized equipment. We focus on an ethanol concentration in the range of 0−15% in volume, typical in the wine industry.

2. Data, Materials, and Methods

The experimental setup is shown in Fig. 1. It consists of a broadband source (BBS) attached to an optical circulator (OC) attached to a Fabry–Pérot sensor and to an optical spectrum analyzer (OSA). The BBS is manufactured in-house and consists of a 100 mW laser diode (LD, Q-Photonics, model QFBGLD-980-100) emitting at approximately 980 nm and powered with 100 mA delivered by a Keithley 6221 AC/DC current source (not shown). The LD is attached to the 980 nm port wavelength division multiplexer (WDM) to avoid reflection that can damage the LD, followed by an Er-doped fiber that produces a wide spectrum (approximately 1500 to 1600 nm) of coherent light. The optical circulator (OC, model Thorlabs 6015-3) with a band from 1525 to 1610 nm is used to deliver the optical signal coming from the BBS to the Fabry–Pérot sensor located in a vial containing the solution being measured, and then to redirect the reflected signals to the OSA.

The Fabry–Pérot interferometer is manufactured with a standard SM28 Corning single-mode optical fiber spliced to a length of the coreless (CL) fiber model Thorlabs FG125LA. Figure 2(a) shows the CL fiber and the SM28 fiber mounted in Fitel splicer model S179 before splicing, whereas Fig. 2(b) shows the two lengths of the fiber spliced together. Eleven interferometers

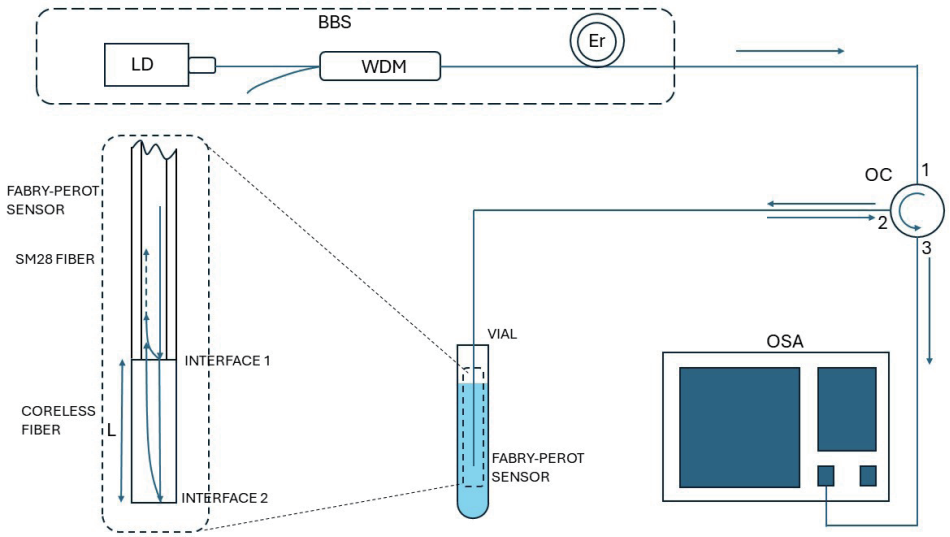

Fig. 1. (Color online) Experimental setup.

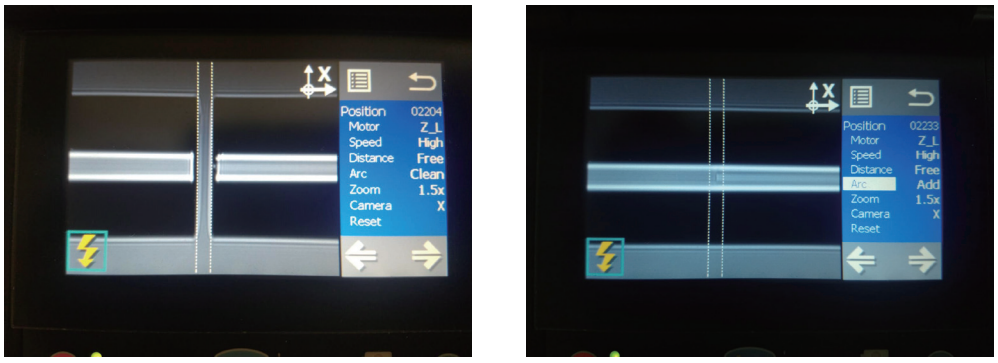

(a) (b)

Fig. 2. (Color online) (a) CL fiber (left-hand side) and SMF (right-hand side) before splicing, and (b) CL fiber and SM28 after splicing.

were assembled with the Fitel splicer using the following parameters: an arc power of 120, a duration of 750 ms, and a *z*-push of 10 mm. Additional discharges were delivered to the spliced section until a homogeneous splice was obtained. After splicing, the coreless fiber was cleaved to the desired length L = 0, 5, 10, …, 50 mm using a ruler incorporated into the fiber cleaver (Fitel S326). The sensor was then inserted into a syringe needle piercing a rubber stopper that is used to cap the vial containing the solution being measured [see vial in Fig. 3(a)]. The fiber optic sensor was held in place using a putty-like compound at the top of the needle, which allowed us to easily adjust the position of the sensor in the vial to ensure that it was fully immersed in the liquid.

The manufactured Fabry–Pérot interferometers provide the following reflection interfaces (see Fig. 1): interface 1 at the SM-coreless fiber interface and interface 2 at the liquid-cleaved end of the coreless fiber. Part of the incoming light is reflected at interface 1, and part is transmitted into the coreless fiber. The transmitted light travels in the coreless fiber for a length $2L$ interacting with the surrounding environment (liquid in our case) via the evanescent wave, and then enters the core of the SM fiber interfering with the light reflected at interface 1. As a first approximation, neglecting multiple reflections between interfaces 1 and 2, the Fabry–Pérot interferometer can be treated as a two-beam interferometer with intensity $I(\lambda)$.[9]

$$I(\lambda) = I_1 + I_2 + 2\sqrt{I_1 I_2}\cos\left(\frac{4\pi r_{eff}\,2L}{\lambda} + \phi_0\right) \tag{1}$$

Here, $I(\lambda)$ is the intensity of the measured beam at wavelength λ, I_1 and I_2 are the intensities of the light beams reflected at interfaces 1 and 2, respectively, $2L$ is the difference between the lengths of the two paths, ϕ_0 is the initial phase difference between the two beams, and r_{eff} is the effective refractive index of the coreless fiber.

Finally, the OSA (Yokogawa, AQ 6370D) receives the interfering beams coming from the sensors and records intensity [dBm] vs wavelength [nm]. After several trials, the parameters of

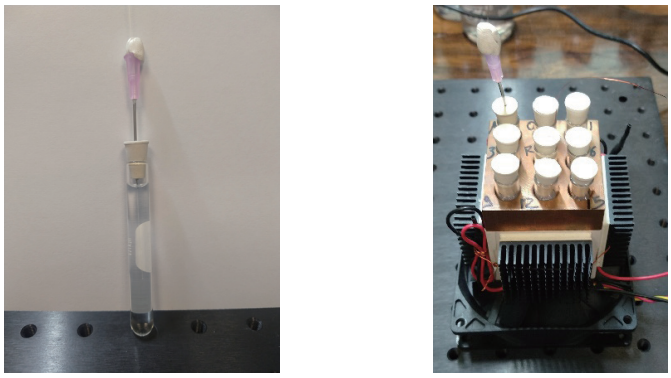

(a) (b)

Fig. 3. (Color online) (a) Sensor inserted into a vial with a solution. (b) Temperature-controlled copper block that can accommodate up to 9 vials. Peltier cells and heat dissipators are visible on the sides of the block.

the OSA were set to the following: resolution = 1 nm, sensitivity = HIGH 1, and average = 2.

Since the speed of the beam in the coreless fiber is affected by the refractive index of the surrounding medium, a variation of the solution refractive index caused by a variation of ethanol content induces a variation of the interference pattern. Therefore, a correlation between the ethanol concentration and the interference pattern registered with the OSA can be found, and the sensor can be calibrated.

To control the temperature of the solutions, the vials were inserted into a temperature-controlled copper block [see Fig. 3(b)] that can accommodate up to 9 vials in a 3 × 3 pattern. The cooling power was provided by four air-cooled Peltier cells glued onto the sides of the copper block and controlled with a Eurotherm 3216 PID system. To minimize the temperature difference between the solutions and the reference temperature measured with a K-type mini-thermocouple, the thermocouple was inserted into a water-filled vial located at the center of the copper block. The remaining vials contained air and the solutions of n% ethanol in deionized (DI) water, with n = 0, 1, 3, 6, 9, 12, and 15. The temperatures at which the measurements were carried out were 23, 21, and 19 °C; once the target temperature was reached, 5 min was given to allow the temperature to stabilize, and all the measurements were conducted with a temperature variation of less than 0.05 °C from the set value.

The solutions were prepared by mixing the appropriate amounts of ethanol and water, and stored in closed hermetic containers. The solutions at a fixed temperature were measured in a single day, ensuring that the vials that were not being measured were capped to minimize evaporation and maintain the nominal concentration of the solutions. Fresh solutions were used every day when measuring at a new temperature.

As an example, we show in Fig. 4(a) the interferometric pattern of a 50-mm-long Fabry–Pérot interferometer at the temperature of 23 °C in H_2O, and in Fig. 4(b) its fast Fourier transform (FFT). The large peaks located at about 0.02 and 0.04 nm^{-1} are indicative of beam interferences at different λ values.

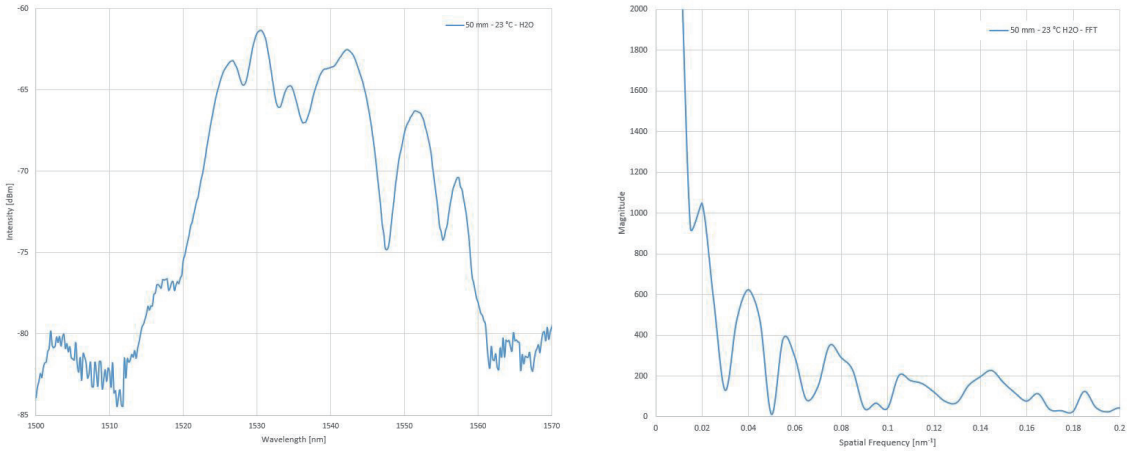

(a) (b)

Fig. 4. (Color online) (a) Interferometric data of a 50-mm-long Fabry–Pérot interferometer held at 23 °C in air. (b) FFT of data above, showing main peaks at about 0.02 and 0.04 nm^{-1}.

3. Results and Discussion

The spectra of all the sensors measured at each operating temperature and ethanol concentration are acquired with the OSA. The position and intensity of all the peaks and valleys of the interference patterns were fitted with a linear function versus the n of the ethanol concentration, and the slope of such a fit (i.e., the sensitivity of the sensor) and the goodness of their linear fit (residual) were taken as discriminating parameters to select the sensors with the highest sensitivity and linearity in the full range $n = 0–15$. Table 1 shows the highest sensitivity (with a ± sign), the length L of the sensor, the temperature at which the measurement was made, and the residual value of the linear fit. For the sensor based on a change in peak/valley intensity, we report also the wavelength interval at which the peak and valley were measured since this information cannot be deduced by the intensity-vs-n graphs. The top half of Table 1 shows the highest shift in peak or valley position per unit change in n, confirming that the sensor is indeed based on an interferometer.

From the analysis of the sensitivity of the peak or valley position in Table 1, we observed that the highest sensitivity [0.07630 (nm/n)] was obtained with a 20-mm-long sensor at 21 °C with good linearity (residual of 0.02592). In Fig. 5, we show the spectra measured with such an interferometer when immersed in the solutions and how the position of the valley located at about 1545 nm changes with ethanol concentration.

In Fig. 6, we show the plot of the peak or valley position vs ethanol concentration of the 20-, 30-, and 45-mm-long interferometers at 21, 23, and 21 °C, all showing good linearity in the range $n = 0–15$.

The bottom half of Table 1 shows the highest shift in peak or valley intensity per unit change in n; we note that the highest signed sensitivity [−0.15696 (dBm/n)] was obtained with a 45-mm-long sensor, at 21 °C, and with good linearity (residual 0.13807). In Fig. 7, we show the measured spectra of such an interferometer when immersed in the solutions and how the position of the peaks located at 1534–1535 nm lowers with ethanol concentration. In Fig. 8, we show the plot of

Table 1
Sensitivity values obtained by fitting the position and intensity of the peaks and valleys vs n for $n = 0-15$.

Peak or valley position			
Sensitivity (nm/n)	Length L (mm)	Temperature (°C)	Residual
0.07630	20	21	0.02592
0.07032	30	23	0.05135
0.06413	45	21	0.06070
Peak or valley intensity			
Sensitivity (dBm/n)	Position (nm)	Length L (mm)	Temperature (°C)	Residual
−0.15696	1534–1535	45	21	0.13807
0.15328	1523–1524	45	19	0.10786
−0.14453	1563–1565	40	19	0.05016

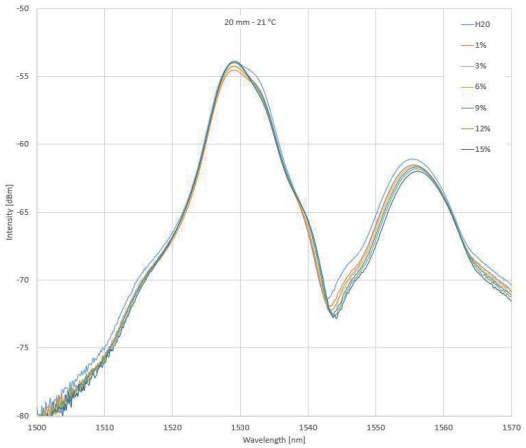

Fig. 5. (Color online) Interferometric data of 20-mm-long interferometer at 21 °C.

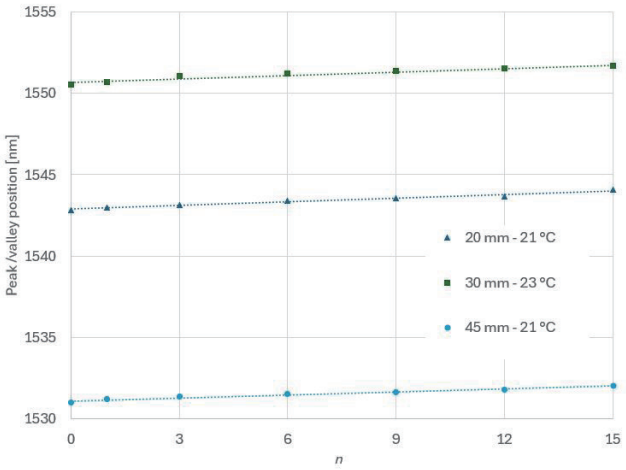

Fig. 6. (Color online) Data points and their linear fit for the interferometers mentioned in Table 1.

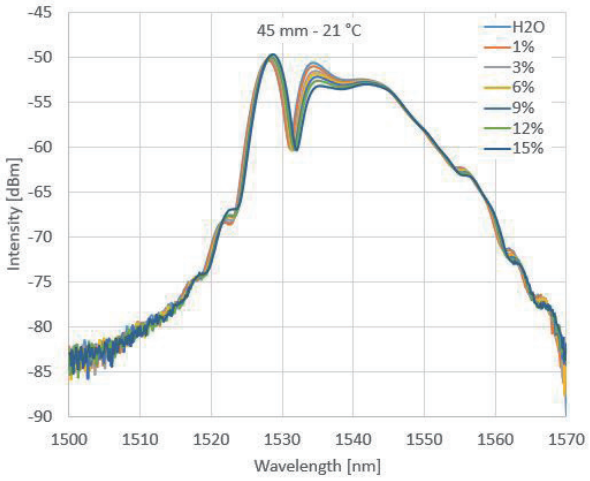

Fig. 7. (Color online) Interferometric data of 45-mm-long interferometer at 21 °C.

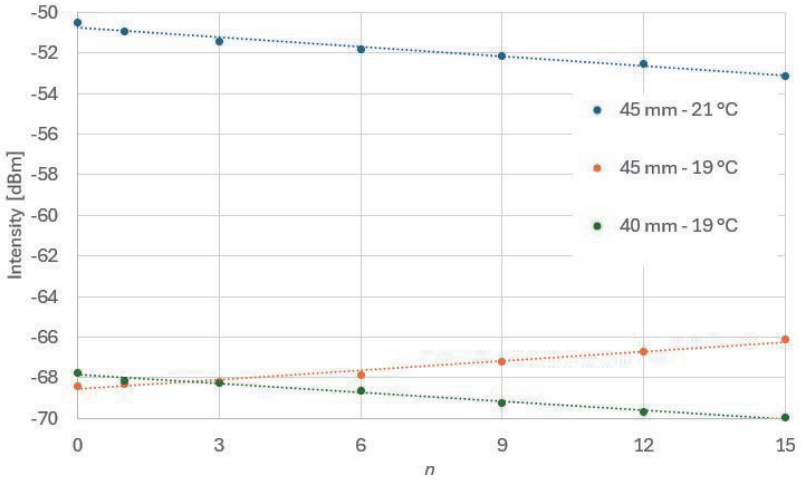

Fig. 8. (Color online) Linear fit of the peak and valley intensities of the interferometers reported in Table 2.

the peak intensity vs ethanol concentration of the 45-mm-long interferometer at 21 and 19 °C, and of the 40-mm-long interferometer at 19 °C, all showing good linearity in the range $n = 0–15$.

We note that the intensity of the valley located at 1523–1524 nm of the 45-mm-long interferometer at 19 °C is increasing, while that of the peak located at 1534–1535 nm of the same interferometer at 21 °C is decreasing. This is not due to the difference in temperature; in fact, in Fig. 7, the intensities of the valleys located at 1523–1524 nm are also increasing with n, while those of the peaks at 1534–1535 nm are decreasing with increasing n, and the temperature is 21 °C in both cases. We believe that the change from an increasing valley intensity in the range of 1523–1524 nm to a decreasing peak intensity in the range of 1534–1535 nm is due to the change in the slope of the cosine function of Eq. (1) when the wavelength changes from the first interval to the second and to the interaction of the evanescent wave with solutions of increasing refractive index. This change in slope is maintained when changing from 21 to 19 °C; in fact, at 19 °C, the

intensity of the peak located in the range of 1534–1535 nm still decreases when n increases (not shown).

In Table 2, we compare the highest sensitivity obtained in this work and measured in nm/n with the sensitivity values reported in the literature. As shown, the sensor reported in this work provides a higher sensitivity and is easier to manufacture than the FBG-based sensors reported by Raikar *et al.*[11] and Terada *et al.*[12]

To compare the sensitivity obtained with our sensor with those found in the literature using the absorbance A, we transformed the intensity from dBm to mW and then defined the absorbance A as $A = \log_{10}(p_0/p_n)$, where P_0 is the power measured with the sensor in pure DI water and P_n is the power measured with the sensor immersed in an n% solution of ethanol in DI water (see Table 3).

In Table 4, we compare the highest sensitivity values obtained in this work and measured in dBm/n and A/n with the sensitivity values found in the literature. The sensor proposed in this work is about 5 times more sensitive in a wider n range than that proposed by Marfu'ah *et al.*.[5] Again, note that the sensors reported by Ji *et al.*,[13] Girei *et al.*,[14] or Li *et al.*[16] are more difficult to manufacture or use expensive photonic fibers when compared with the sensor reported in this work.

Table 2
Sensitivity values measured in nm/n found in literature.

Reference	Sensitivity (nm/n)	Range (n)
6	0.9399	0−15
10	0.28	30−70
This work	0.07630	0−15
12	−0.013	0−70
11	0.002	0−50

Table 3
Sensitivity measured in A/n obtained in this work.

Sensor length (mm)	Temperature (°C)	Sensitivity (dBm/n)	Sensitivity (A/n)
45	21	−0.15696	0.0157

Table 4
Comparison of the highest sensitivity values obtained in this work measured in dBm/n or A/n with the sensitivity values found in the literature.

Reference	Sensitivity (dBm/n)	Sensitivity (A/n)	Range (n)
This work	−0.15696	–	0−15
5	0.028972	–	0−10
15	–	0.0755	0−18
This work	–	0.0157	0−15
13	–	0.00461	0−100
16	–	0.0034	0−100
14	–	0.00133	0−40

4. Conclusions

In this work, we designed and tested fiber optic sensors based on a Fabry–Pérot interferometer to measure the concentration of ethanol in DI water solutions in the range of 0–15% typical in the wine industry. Our design uses a Corning SM-28 fiber spliced without offset to CL fibers with lengths of $L = 0, 5, 10, \ldots, 50$ mm. The interference patterns obtained from the sensors immersed in the solutions at temperatures of 19, 21, and 23 °C were analyzed and the highest sensitivity values obtained were 0.07630 nm/n and −0.15696 dBm/n in the range $n = 0$−15 with good linearity. Although they are simple in construction, the sensors are sensitive to the temperature of the sample and require the thermal control of the solutions being measured.

Acknowledgments

This work was supported by the IDEA-GTO and CNR partnership that financed this work via the project "Correlation of physicochemical and sensory properties to the response of nanofunctionalized fiber optic sensors in wines produced in Guanajuato" with grants IDEAGTO/CONV/13/2022 in México and 101016706 — h-ALO — H2020-ICT-2018-20/H2020-ICT-2020-2 in Italy. MB and MSAG wish to thank Mr. J Antonio Ávila Gutierrez for his help in setting up the laboratory.

References

1 Ethanol Uses, Benefits, and Chemical Safety Facts. https://www.chemicalsafetyfacts.org/ethanol/
2 S. F. Memon, R. Wang, B. Strunz, B. S. Chowdhry, T. T. Pembroke, and E. Lewis: Sensors **22** (2022) 950. https://doi.org/10.3390/s22030950
3 P. M. Thirunavakkarasu, A. A. Khan, A. S. M. Noor, N. Saidin, and A. Waqas: Opt. Fiber Technol. **82** (2024) 103584. https://doi.org/10.1016/j.yofte.2023.103584
4 M. S. Cano-Velázquez, A. L. Hendriks, L. Picelli, R. P. J. van Veldhoven, and A. Fiore: Sensors **23** (2023) 7703. https://doi.org/10.3390/s23187703
5 Marfu'ah, R. A. Niza, M. H. Agus, and Y. P. Detak: AIP Conf. Proc. **1945** (2018) 20031. https://doi.org/10.1063/1.5030253
6 J. Tian, M. Quan, Y. Jiao, Y. Yao, W. Liang, Y. Y. Huang, Y. Xu, R. K. Lee, and A. Yariv: Opt. Express **24** (2016) 20132. http://dx.doi.org/10.1364/OE.24.020132
7 T. Paixão, A. S. Nunes, J. Bierlich, J. Kobelke, and M. S. Ferreira: Appl. Sci. **12** (2022) 726. https://doi.org/10.3390/app12020726
8 W. Naku, C. Zhu, A. K. Nambisam, R. E. Gerald II, and J. Huang: Opt. Express **24** (2021) 40000. https://doi.org/10.1364/OE.441144
9 Y. J. Rao: Opt. Fiber Technol. **12** (2006) 227. https://doi.org/10.1016/j.yofte.2006.03.004
10 C. Liao, F. Zhu, P. Zhou, Y. Wang, and H. Kong: Micromachines **10** (2019) 741.
11 U. S. Raikar, V. K. Kulkarni, A. S. Lalasangi, K. Madhav, and S. Asokan: Optoelectron. Adv. Mater.-Rapid Commun. **1** (2007) 149.
12 G. G. Terada, G. R. C. Possetti, E. Camilotti, H. J. Kalinowski, J. L. Fabris, and M. Muller: SBMO/IEEE MTT-S Int. Microwave and Optoelectronics Conf. (Belem, Brazil, 2009) 629–633; https://doi.org/10.1109/IMOC.2009.5427505
13 L. Ji, M. Wenying, Y. Jun, E Weimin, and L. Quiao: Key Eng. Mater. **885** (2014) 609. https://doi.org/10.4028/www.scientific.net/KEM.609-610.885.
14 S. H. Girei, A. A. Shabaneh, H. Ngee-Lim, M. N. Hamidon, M. A. Mahdi, and M. H. Yaacob: Opt. Rev. **22** (2015) 385. https://doi.org/10.1007/s10043-015-0075-8
15 R. C. Tarca, A. M. Caraban, S. Bota, I. C. Tarca, A. Dergez, and A. C. Cozma: Rev. Chim. (Bucarest) **65** (2014) 1238.
16 Z. Li, C. Zhang, Y. Han, S. Gao, Y. Sheng, S. Zhang, Z. Lu, B. Man, Y. Jiao, and S. Jiang: J. Phys. D Appl. Phys. **50** (2017) 315302.